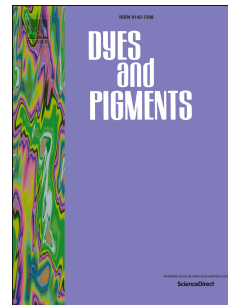


Accepted Manuscript

Synthesis and thermal properties of arylazo pyridone dyes

Slavica J. Porobić, Aleksandar D. Krstić, Dragana J. Jovanović, Jelena M. Lađarević, Đurica B. Katnić, Dušan Ž. Mijin, Milena Marinović-Cincović



PII: S0143-7208(19)31055-1

DOI: <https://doi.org/10.1016/j.dyepig.2019.107602>

Article Number: 107602

Reference: DYPI 107602

To appear in: *Dyes and Pigments*

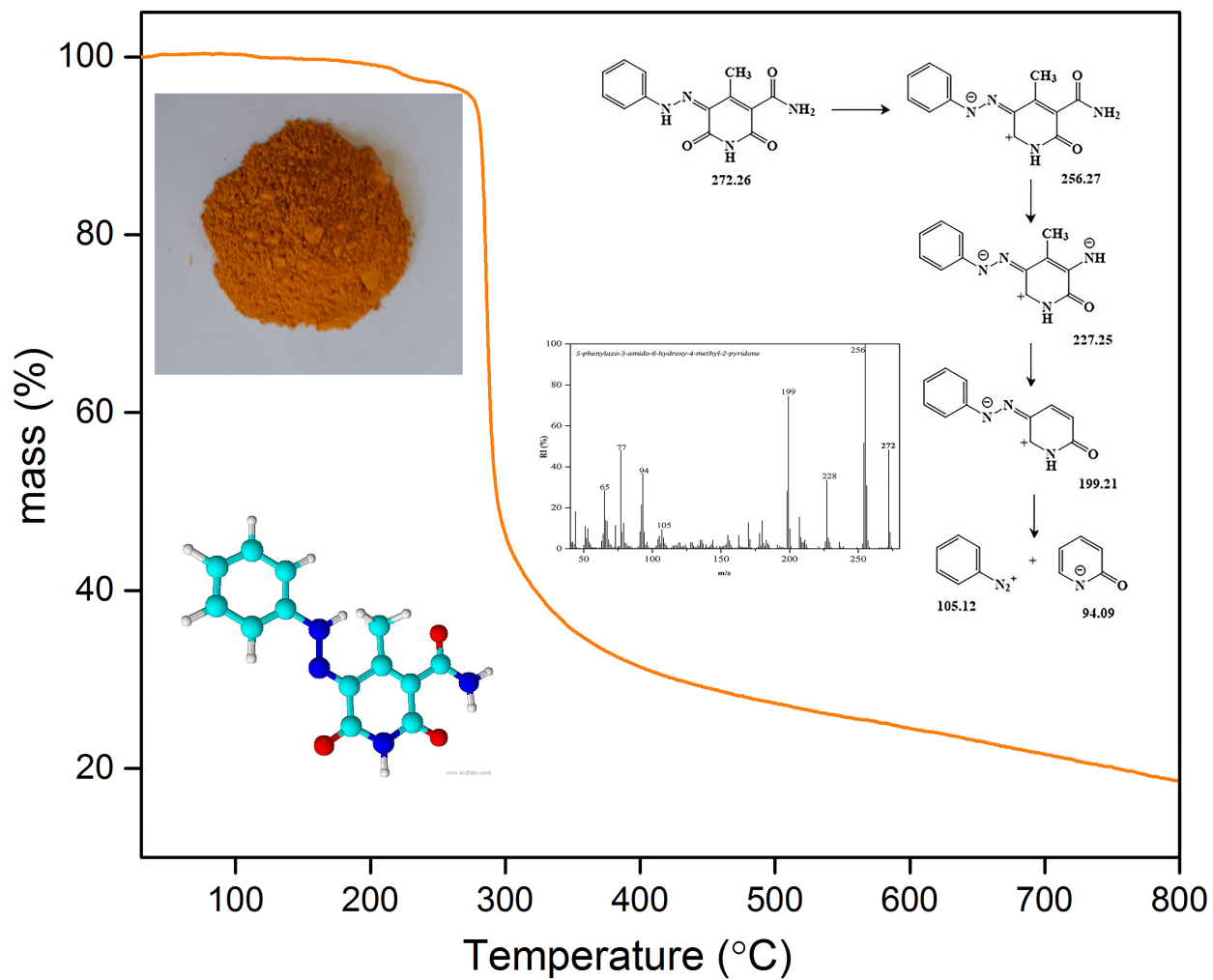
Received Date: 9 May 2019

Revised Date: 30 May 2019

Accepted Date: 30 May 2019

Please cite this article as: Porobić SJ, Krstić AD, Jovanović DJ, Lađarević JM, Katnić ĐB, Mijin Duž, Marinović-Cincović M, Synthesis and thermal properties of arylazo pyridone dyes, *Dyes and Pigments* (2019), doi: <https://doi.org/10.1016/j.dyepig.2019.107602>.

This is a PDF file of an unedited manuscript that has been accepted for publication. As a service to our customers we are providing this early version of the manuscript. The manuscript will undergo copyediting, typesetting, and review of the resulting proof before it is published in its final form. Please note that during the production process errors may be discovered which could affect the content, and all legal disclaimers that apply to the journal pertain.



Slavica J. Porobić^a, Aleksandar D. Krstić^b, Dragana J. Jovanović^a, Jelena M. Lađarević^c, Đurica B.

Katnić^b, Dušan Ž. Mijin^c, Milena Marinović-Cincović^{a,*}

^aUniversity of Belgrade, Institute of Nuclear Sciences "Vinča", Laboratory for Radiation Chemistry and Physics, "Gamma", Mike Petrovića Alasa 12-14, P.O. Box 522, 11001 Belgrade, Serbia

^bUniversity of Belgrade, Institute of Nuclear Sciences "Vinča", Department of Physical Chemistry, Mike Petrovića Alasa 12-14, P.O. Box 522, 11001 Belgrade, Serbia

^cUniversity of Belgrade, Faculty of Technology and Metallurgy, Department of Organic Chemistry, Karnegijeva Street 4, 11120 Belgrade, Serbia

Abstract

Thermal degradation properties of 5-(4-substitutedphenylazo)-3-amido-6-hydroxy-4-methyl-2-pyridones and 5-(4-substitutedphenylazo)-3-cyano-6-hydroxy-4-methyl-2-pyridones dyes, differing in electron withdrawing and electron donating substituents in *para*- position of diazo components were examined. The structure of the synthesized compounds has been confirmed by ¹H NMR, ¹³C NMR, FTIR, UV-Vis and XRD analysis techniques. The results obtained with thermogravimetric analysis (TGA) – derivative thermogravimetry (DTG) and differential thermal analysis (DTA) were combined with GC-mass spectral fragmentation to obtain thermal decomposition mechanism. Non-isothermal kinetics were monitored by application of TGA-DTG-DTA. For Kinetic behavior of the investigated dyes during their degradation in an inert atmosphere, Kissinger, Ozawa, Flynn-Wall-Ozawa (FWO) and Kissinger-Akahira-Sunose (KAS) isoconversional (model-free) methods were applied. It was found that different thermal stabilities of investigated dyes are the consequence of their different chemical structures, including diverse substituents.

Keywords: Azo dyes; Degradation; Thermal stability; Kinetics behavior

*Corresponding Author

E-mail address: milena@vinca.rs (M. Marinović-Cincović).

Azo dyes represent a large class of compounds with wide industrial applications such as optical data storage, dye-sensitized solar cells, laser technology, ink-jet printers, non-linear optics and colorimetric sensors [1-9]. Also, they have found application in the textile and pharmaceutical industry [9-13]. Heterocyclic azo dyes are preferred over carbocyclic azo dyes due to prominent bathochromic effect. Heterocyclic azo compounds containing S and N atoms have shown potential applications in a number of biological reactions. Furthermore, these dyes are environmentally friendly [14-17].

The significance of azo dyes is reflected in a simple preparation by diazotization and azo coupling, and possibilities of combining many different diazo compounds and coupling components in order to obtain a large number of dyes of different colors and characteristics [18].

An important group of azo dyes is based on pyridone derivatives as coupling components [18-20]. These dyes have excellent coloration properties and give bright yellow-red hues. The utilization of the dyes for special uses is associated with their thermal stability. Depending on the nature of substituent (electron withdrawing or electron donating) that is located on the *para*- position of the diazo components of azo pyridone dyes, different thermal stability can be obtained [21].

The results of the thermal analysis of arylazo dyes can be used to obtain useful information about their thermal stability and also to determine the temperature range in which they can be used without changes in their composition, color and properties.

The resistance to heat at elevated temperatures is one of the main properties required of dyes used in high-temperature processes such as dyeing, printing and in high technology areas such as lasers and electro-optical devices [21-28]. The kinetics of thermal degradation of dyes is an important factor in describing the impact of experimental parameters included in the characterization procedure or in the synthesis routes on the parameters which are related to the reactivity of dyes, in given conditions that would dictate their application [29-34].

In this work, three new 5-(4-substituted phenylazo)-3-amido-6-hydroxy-4-methyl-2-pyridone dyes were synthesized in order to examine their thermal stability and kinetic behavior, and compare them

with the same quantities of their 3-cyano analogs that were previously synthesized by Ušćumlić et al. [35, 36].

The structures of the synthesized compounds have been confirmed by elemental analysis, FTIR, NMR, UV-Vis and XRD analysis, and thermal stability is examined using TGA-DTG and DTA techniques. According to our best knowledge, the kinetics behavior from generic standpoints for these synthesized pyridone dyes with established kinetic parameters (such as activation energy, E , and pre-exponential factor, Z) is not reported in the open literature. Toward a kinetic analysis of the synthesized azo dyes, a certain number of selected non-isothermal kinetic methods were applied.

2. Experimental

2.1. Materials

2-Cyanoacetamide (99%), Acros; ethylacetoacetate, Fluka; methanol (>99.99 %), Acros; potassium hydroxide, Hemoss; hydrochloric acid, Merck; sulfuric acid, Zorka Šabac; aniline (>98%), Fluka; *p*-bromoaniline (>98%), Fluka; 4-aminophenol (>97%), Fluka; sodium nitrite, Hemoss; ethanol, HPLC, Fisher Chemical; DMSO (>97 %), Merck.

2.2. Synthesis

All investigated azo dyes have been synthesized from the corresponding diazonium salts and 3-amido-6-hydroxy-4-methyl-2-pyridone (**1a-c**) or 3-cyano-6-hydroxy-4-methyl-2-pyridone (**2a-c**) using the classical reaction of diazotization and diazo-coupling for the synthesis of the azo compounds [37]. The crude products were recrystallized from *N,N*-dimethylformamide.

2.2.1. Synthesis of 3-cyano-6-hydroxy-4-methyl-2-pyridone

3-Cyano-6-hydroxy-4-methyl-2-pyridone has been prepared as published before [38]. The 2-Cyanoacetamide (5 g, 0.06 mol), ethyl acetoacetate (7.8 g, 0.06 mol) and potassium hydroxide (3.92 g, 0.07 mol) of were dissolved in methanol (120 mL). A homogeneous mixture was heated with stirring for 8 hours in a flask equipped with an Allihn condenser. By filtration on the Büchner funnel, the solid was separated, which was then dissolved in distilled water. Concentrated hydrochloric acid

ACCEPTED MANUSCRIPT
was added to the solution to give an acidic medium. Then, the solid substance was separated by filtration on the Büchner funnel, and it was dried in the air.

2.2.2. Synthesis of 3-amido-6-hydroxy-4-methyl-2-pyridone

In order to convert 3-cyano-6-hydroxy-4-methyl-2-pyridone to 3-amido-6-hydroxy-4-methyl-2-pyridone, acid hydrolysis was done using the following procedure: 3-cyano-6-hydroxy-4-methyl-2-pyridone (1.0 g, 6.67 mmol) was added carefully to 10 mL of sulphuric acid (with 15% of SO₃). The reaction temperature was maintained below 100 °C. Then, the reaction mixture was heated for 30 min using a water bath at 95–100 °C and after that the mixture was poured over 200 g of crushed ice. The obtained crystals were isolated by filtration and dried on air. The structure of 3-amido-6-hydroxy-4-methyl-2-pyridone is confirmed by the following characteristics: white crystalline substance; m.p.196–197°C, yield 42%; FT-IR (KBr, v/cm⁻¹): 3482 (NH), 3419 (OH), 1670, 1623 (C=O), 1557 (NH), 1430 (C–N), 708 (NH); ¹H NMR (200 MHz, DMSO-*d*₆, δ/ppm): 2.38 (3H, s, CH₃), 5.52 (1H, s, C₅); ¹³C NMR (50 MHz, DMSO-*d*₆, δ/ppm):169.97, 164.70, 159.37, 156.14, 101.74, 99.82, 23.14.

2.2.3. Preparation of the diazonium salt

The corresponding aniline was dissolved in concentrated hydrochloric acid (2.5 mL) and cooled down to 0 °C. Sodium nitrate (11 mmol) was dissolved in cold water (4 mL) and added dropwise to the aniline solution. The mixture was stirred for an hour to give the diazonium salt of the corresponding aniline [39].

2.2.4. Synthesis of 5-(4-substitutedphenylazo)-3-amido-6-hydroxy-4-methyl-2-pyridones (**1a-c**) and 5-(4-substitutedphenylazo)-3-cyano-6-hydroxy-4-methyl-2-pyridones (**2a-c**)

The corresponding pyridone (10 mmol) was dissolved in an aqueous potassium hydroxide solution and cooled down to 0 °C. Then diazonium salt of selected aniline was added dropwise to a solution of pyridone which was stirred for half an hour. Additionally, the mixture was stirred for 3 hours while maintaining a low temperature (0 °C). Further, the mixture was left in the fridge

overnight, after that, it was filtered, washed with water and dried. The compounds were recrystallized using *N,N*-dimethylformamide, and the solid substance is separated by filtration on the Büchner funnel. Obtained dyes were dried in the air. The overall synthesis scheme is presented in Fig. 1.

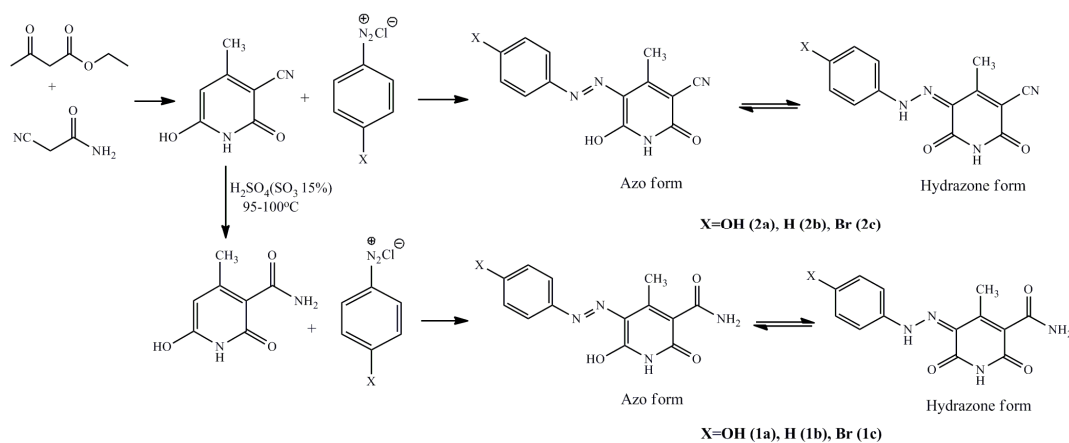


Fig. 1. The dyes synthesis scheme and their azo-hydrazone tautomerism.

2.3. Methods of characterization

Elemental analysis was performed using a Vario EL III elemental analyzer.

2.3.1. FT-IR, NMR

The IR spectra were recorded using a Bomem (Canada) MB-Series 100 Fourier transform-infrared (FT-IR) spectrophotometer in the form of KBr pellets. The ¹H and ¹³C NMR data were performed using a Varian Gemini 2000 (200 Hz and 50 Hz, respectively) in deuterated dimethyl sulfoxide (DMSO-*d*₆) and trifluoroacetic acid (CF₃COOD) with tetramethylsilane (TMS) as an internal standard. All spectral measurements were carried out at room temperature (25 °C).

2.3.2. UV/Vis spectra

The ultraviolet-visible (UV/Vis) absorption spectra were recorded on a Shimadzu UV-Visible UV-2600 (Japan) spectrophotometer in the range 200-700nm.

Azo dyes were examined by X-ray powder diffraction. XRD measurements were performed using a Rigaku (Japan) SmartLab diffractometer with X-ray lamp working on 40V/30mA. Diffraction data were recorded in a 2θ range from 10° to 60° counting 10°min^{-1} in 0.02° steps.

2.3.4. Thermogravimetric (TG) and derivative thermogravimetry (DTG) studies

The thermal stability of the samples was investigated by the TGA and DTG techniques, as well as DTA technique, using a Setaram Setsys Evolution 1750 instrument (France). The samples were heated from 30 to 800°C in a flow rate of $\varphi = 20\text{ cm}^3\text{ min}^{-1}$, under the pure argon (Ar) with a heating rate of $\beta = 2.5, 5, 10$ and $20^\circ\text{C min}^{-1}$. For thermal characterization purposes of the studied samples, thermo-analytical curves at $10^\circ\text{C min}^{-1}$ were only displayed. The average mass of the samples was about 4 mg.

2.3.5. Gas chromatography-mass spectrometry (GC-MS)

For GC/MS analysis Agilent Technologies 7890B gas chromatograph coupled with 5977 MSD mass detector was used. The gas chromatograph was equipped with a capillary column HP-5 MS Inert ((5% phenyl)-methylpolysiloxane, $30\text{m} \times 0.25\text{ mm}$, film thickness $0.25\ \mu\text{m}$ from Agilent technologies). For data processing MassHunter Qualitative analysis software from Agilent Technologies was used. The injector was operated at 280°C . The oven temperature was raised from 150°C to 305°C at a heating rate $5^\circ\text{C per minute}$ and isothermally hold 10 minutes. As a carrier gas helium at 0.9 ml min^{-1} was used. Injection volume was $1\ \mu\text{l}$. Samples were dissolved in dimethylformamide (DMF) (1:1000) and injected in a splitless mode. Mass detector was operated at the ionization energy 70 eV in the $40\text{-}550\text{ amu}$ range, threshold was 150 amu and speed scanning of 1.56 u/s .

3. Results and discussion

3.1. FTIR and ^1H NMR results

The investigated dyes exhibit azo-hydrazone tautomerism (Figure 1), due to the presence of the –OH group in the *ortho*- position to the azo bridge [35].

The IR and ^1H NMR data for the synthesized arylazo pyridone dyes are given in Table 1. Elemental analysis and ^{13}C NMR spectral data of dyes **1a-c** are given in Table 2. The IR and NMR spectra of the dyes clearly show the existence of the hydrazone form in powder form and DMSO- d_6 , respectively. The infrared spectra of **1a**, **1b** and **1c** dyes (Table 1) showed characteristic vibrations of two carbonyl group in the region of ν_{CO} 1643–1673 cm^{-1} indicating the hydrazone tautomeric form. Also, N–H stretching vibrations from hydrazone group are observed the region 3436–3457 cm^{-1} , while N–H stretching of pyridone moiety is noted in the region of 3129–3164 cm^{-1} . The infrared spectra of **2a**, **2b** and **2c** dyes (Table 1) also showed the presence of the hydrazone form: two carbonyl stretching vibrations (1648–1674 cm^{-1}), N–H hydrazone stretching (3385–3390 cm^{-1}), N–H stretching from pyridone ring (3141–3153 cm^{-1}). Sharp peaks at 2224–2230 cm^{-1} are attributed to –CN group [36].

The ^1H NMR spectra of all dyes (Table 1) exhibit a broad signal near 14.14–14.87 ppm. This signal corresponds to N–H proton resonance of the hydrazone form. These experiments are in agreement with the previously reported results [35,40]. Also, ^{13}C NMR spectra of the **1a-1c** dyes confirmed the existence of the hydrazone form. Peaks observed in the region 166.5–166.9 ppm are ascribed to carbonyl group of 3-amido, while peaks from originating from pyridone ring are observed at 161.9–162.2 ppm. The signals at 134.1 (**1a**), 126.0 (**1b**) and 126.5 (**1c**) are ascribed to hydrazone C=N group.

Table 1. IR and ¹H NMR spectral data of synthesized arylazo pyridone dyes

Dye	IR (KBr) ν (cm ⁻¹)			¹ H NMR (200 MHz, DMSO- <i>d</i> ₆ , δ (ppm))
	ν_{CN}	ν_{NH}	ν_{CO}	
1a	/	3436, 3129	1670, 1643	2.23 (3H, s, CH ₃), 6.85 (2H, d, <i>J</i> = 8.0 Hz, Ar-H), 7.41 (2H, d, <i>J</i> = 8.0 Hz, Ar-H), 7.48 (1H, s, NH ₂), 7.68 (1H, s, NH ₂), 9.68 (H, s, OH), 11.56 (1H, s, NH on heterocyclic), 14.48 (1H, s, NH of hydrazone form)
1b	/	3457, 3164	1673, 1656	2.23 (3H, s, CH ₃), 7.20 (1H, t, <i>J</i> = 7.0 Hz, Ar-H), 7.36-7.60 (5H, m, NH ₂ +Ar-H), 7.71 (1H, s, NH ₂), 11.68 (1H, s, NH on heterocyclic), 14.25 (1H, s, NH of hydrazone form)
1c	/	3445, 3148	1673, 1653	2.21 (3H, s, CH ₃), 7.50 (2H, d, <i>J</i> = 10.0 Hz, Ar-H), 7.51 (1H, s, NH ₂), 7.60 (2H, d, <i>J</i> = 8.0 Hz, Ar-H), 7.69 (1H, s, NH ₂), 11.70 (1H, s, NH on heterocyclic), 14.14 (1H, s, NH of hydrazone form)
2a	2224	3385,3153	1668, 1648	2.50 (3H, s, CH ₃), 6.88 (2H, d, <i>J</i> = 9 Hz, Ar-H), 7.55 (2H, d, <i>J</i> = 9 Hz, Ar-H), 11.93 (1H, s, N-H on heterocyclic), 14.87 (1H, s, N-H of hydrazone form)
2b	2230	3390,3153	1670, 1656	2.76 (3H, s, CH ₃), 7.55 (5H, m, Ar-H), 11.89 (1H, s, N-H on heterocyclic), 14.55 (1H, s, N-H of hydrazone form)
2c	2227	3385,3141	1674, 1665	2.50 (3H, s, CH ₃), 7.51 (2H, d, <i>J</i> = 9 Hz, Ar-H), 7.67 (2H, d, <i>J</i> = 9 Hz, Ar-H), 11.99 (1H, s, N-H on heterocyclic), 14.45 (1H, s, N-H of hydrazone form)

Table 2. Elemental analysis and ¹³C NMR spectral data of arylazo pyridone dyes (**1a-c**)

Dye	Elemental analysis	¹³ C NMR (50 MHz, DMSO- <i>d</i> ₆ , δ /ppm)
1a	C ₁₃ H ₁₂ N ₄ O ₄ : C, 54.17; H, 4.20; N, 19.44 Found: C, 54.01; H, 4.10; N, 19.11	166.9 (CONH ₂), 162.2 (Py), 162.0 (Py), 156.1 (Ar), 146.1 (Py), 134.1 (Ar), 124.0 (C=N), 122.6 (Py), 118.1 (Ar), 116.5 (Ar), 14.5 (CH ₃)
1b	C ₁₃ H ₁₂ N ₄ O ₃ : C, 57.35; H, 4.44; N, 20.58 Found: C, 56.81; H, 4.31; N, 19.77	166.6 (CONH ₂), 162.2 (Py), 162.0 (Py), 145.6 (Py), 142.0 (Ar), 129.9 (Ar), 126.0 (C=N), 125.5 (Ar), 124.0 (Py), 116.3 (Ar), 14.5 (CH ₃)
1c	C ₁₃ H ₁₁ BrN ₄ O ₃ : C, 44.46; H, 3.16; N, 15.95 Found: C, 44.11; H, 3.20; N, 16.12	166.5 (CONH ₂), 162.2 (Py), 161.9 (Py), 145.3 (Py), 141.5 (Ar), 132.6 (Ar), 126.5 (C=N), 124.6 (Py), 118.3 (Ar), 117.2 (Ar), 14.5 (CH ₃)

The UV-Vis spectral data of arylazo pyridone dyes in ethanol [35] are shown in Table 3. The obtained data confirm that the positions of the UV-Vis absorption maxima depend on the nature of the substituents of the diazo component as well as on the nature of the substituents of the pyridone component. Introduction of a donor substituent (–OH) into the diazo component leads to a significant bathochromic shift of the long-wavelength absorption maximum, due to reinforced π -delocalization. From Table 3, it can be noted that introduction of amido group in the position 3 of the pyridone ring instead of cyano causes a hypsochromic shift of absorption maxima of the corresponding dyes. It has been established that for 3-cyano pyridone dyes, cyano group represents the principal acceptor of the charge transfer through the molecule [36,41]. The replacement of this strong electron-accepting group with weaker amido- group causes the change in the transmission mode of electron density which is reflected by afore mentioned hypsochromic shift. Also, CIE lab diagram for dyes **1a-c** and **2a-c** is shown in Fig. 2.

Table 3. The wavelength maxima λ_{\max} (nm) from UV-Vis absorption spectra of arylazo pyridone dyes in ethanol and the molar extinction coefficients

Dye	1a	1b	1c	2a	2b	2c
λ_{\max} (nm)	451.3	420.1	420.2	469.5	433.1	438.5
$\log \epsilon$ ($\text{mol}^{-1}\text{dm}^3\text{cm}^{-1}$)	4.48	4.49	4.56	4.52	4.37	4.32

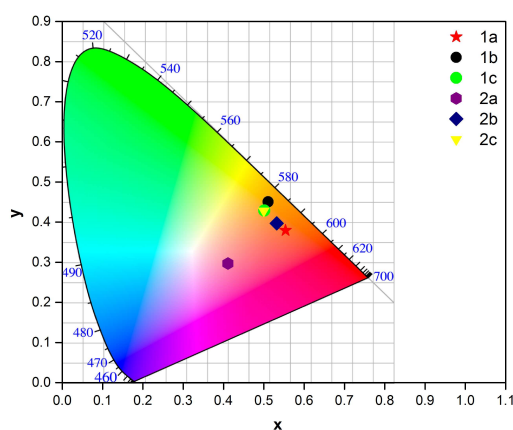


Fig. 2. CIE lab diagram for dyes **1a-c** and **2a-c**

The XRD analysis for all synthesized dyes (Figs. 3a and 3b), showed relatively intense narrow reflection peaks suggesting that the all synthesized dyes are highly crystalline, and no additional thermal treatment is necessary. Aziz et al. [42] also confirmed the crystalline form of azo dyes through the XRD spectra analysis. Arylazo pyridone dyes generally crystallize in hydrazone form [43, 44]. The formation of layered structures is the consequence of hydrogen bonds and π - π stacking interaction. The change of the substituent on the phenyl ring causes a change in the dihedral angle between the plane of the pyridone and the phenyl ring and leads to a different package of molecules.

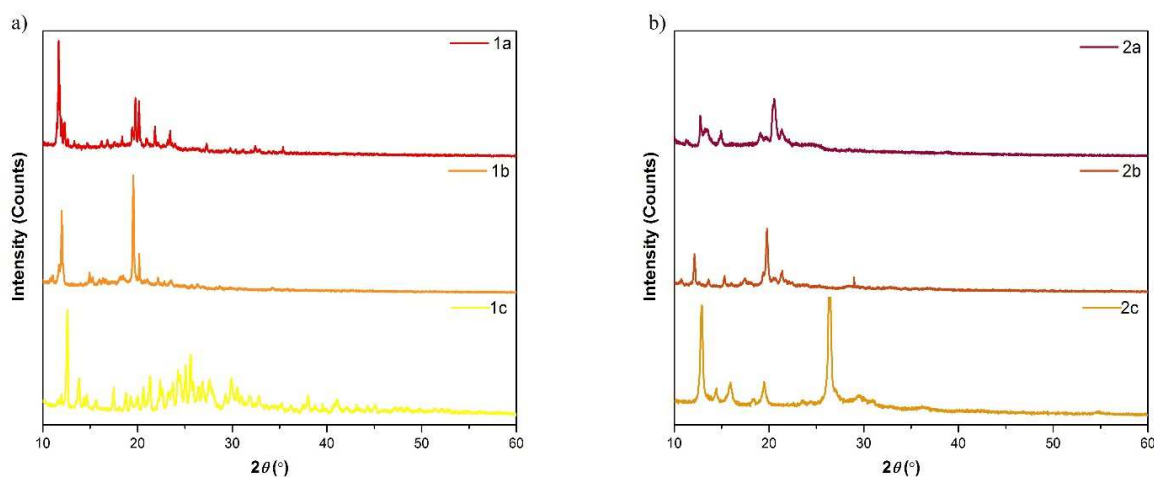


Fig. 3. XRD patterns for dyes: a) **1a**, **1b** and **1c**; b) **2a**, **2b** and **2c**

3.4. Thermal analysis results

Thermal stability of azo dyes was analyzed using TGA-DTG and DTA techniques. The temperature of the beginning of the sample decomposition represents the thermal stability of the investigated dyes. The simultaneous TGA-DTG curves at the heating rate of $10\text{ }^{\circ}\text{C min}^{-1}$ are shown in Figs. 4-9. Based on the mass spectral fragmentation pathways, the degradation of dyes **1a-c** and **2a-c** is assumed. Also, the resulting degradation fragments have been confirmed by FT-IR spectra of the dyes before heating and the residue after heating at specified temperatures.

TGA curve (Fig. 4) of compound **1a** shows that thermal degradation occurs in three steps. The first step (at $50 - 80\text{ }^{\circ}\text{C}$) is due to evaporation of free adsorbed water (4%) which can be seen on DTA curve (Fig. 10) as a peak at $71\text{ }^{\circ}\text{C}$. The second step (at $277 - 400\text{ }^{\circ}\text{C}$) is due to loss of $-\text{C}_6\text{H}_6\text{ON}_2^+$, CO

and NO (Exper. % = 63, Calcd. = 62.5 %) and the third step (at 400 – 800 °C) is due to fragmentation of residual pyridone $C_5H_5NO^+$. These mass losses are observed as two peaks in DTG feature (Fig. 4) at 70 and 305.6 °C, and in DTA curve (Fig. 10) as endothermic peaks at 71 and 305 and 365 °C, respectively.

Compound **1b** shows three degradation steps (Fig. 5): the first step (at 180 – 270 °C) is due to dehydroxylation of chemically bonded water (4%). The second step (at 270 – 425 °C) is due to loss of $-C_6H_5N_2^+$, CO_2 , NO (Exper. % = 65.9, Calcd. = 65.8 %) and the third step is due to the fragmentation of residual pyridone $C_5H_4NO^-$. These mass losses appeared in DTG feature at 285.8 °C (Fig. 5) and at 283.6 °C as endothermic peak observed in DTA curve (Fig. 10).

Compound **1c** shows four degradation steps (Fig. 6): the first step (at 70 – 95 °C) is due to the loss of free adsorbed water (2%), the second step (at 100 – 120 °C) is due to the loss of $-HCN$ (Exper. % = 7.5, Calcd. = 7.7 %), the third step (at 290 – 500 °C) is due to loss of $-C_6H_4BrN_2^+$ and CO_2 (Exper. % = 71.5, Calcd. = 71.0 %). The fourth step (at 500 – 800 °C) is due to residual gaseous compounds. These mass losses appeared in DTG feature at 101.5 and 299.6 °C (Fig. 6) and at 103.3 and 296.9 °C, as two endothermic peaks in DTA curve (Fig. 10).

The degradation of compound **2a** occurs in three steps (Fig. 7): the first step (at about 80 °C) is due to the loss of free adsorbed water (2%), the second step (at 130 – 195 °C) is due to dehydroxylation of chemically bonded water (10%). The third step (at 275 – 700 °C) is due to the loss of $C_6H_5N_2^+$, HCN and CH_4 (Exper. % = 51, Calcd. = 50 %). These mass losses are observed as two peaks in DTG feature (Fig. 7) at 192.1 and 291.6 °C, and in DTA curve as an endothermic peak at 80 and 192 and exothermic peak at 291.7 °C, respectively (Fig. 11).

Compound **2b** shows three degradation steps (Fig. 8): the first step (at 190 – 240 °C) is due to dehydroxylation of chemically bonded water (10%), the second step (at 288–350 °C) is due to loss of $C_6H_5N^+$ (Exper. % = 36, Calcd. = 35.8 %), the third step (at 350 – 800 °C) is due to the slow degradation of residual pyridone $C_7H_5N_3O^+$. These mass losses are observed as three peaks in DTG feature (Fig. 8) at 85 °C (free adsorbed water), 228.7 and 308.2 °C, and in DTA curve as endothermic peaks at 79.5 and 234.6 °C, respectively, and one exothermic peak at 311.1 °C (Fig. 11).

Compound **2c** shows three degradation steps (Fig. 9): the first step at about 85 °C is due to the

loss of free adsorbed water (3%), the second step (at 260 – 320 °C) is due to loss of HBr, HCN and ·OH (Exper. % = 37, Calcd. = 37.5 %) and the third step (at 320 – 700 °C) is due to the loss of C₆H₆ (Exper. % = 23, Calcd. = 23.4 %). These mass losses appeared in DTG feature at a single point of 280.7 °C (Fig. 9) and at 282.1 °C as one exothermic peak in DTA curve (Fig. 11).

The appearance of some endothermic peaks in the DTA curves arises from the chemical reaction of separated gases with residual substance. In all examined dyes, the mass losses linked to the first step were attributed to the elimination of adsorbed water molecules, that exhibits endothermic behavior. Initial degradation of dyes molecule structure occurs in the second degradation step (above 250 °C). The remaining of 10-30% represent some formed carbon-based residues.

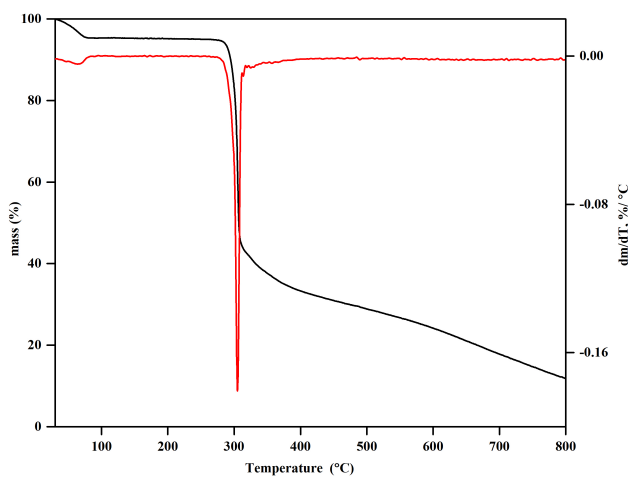


Fig. 4. The TG/DTG curves of dye **1a** at 10 °C min⁻¹

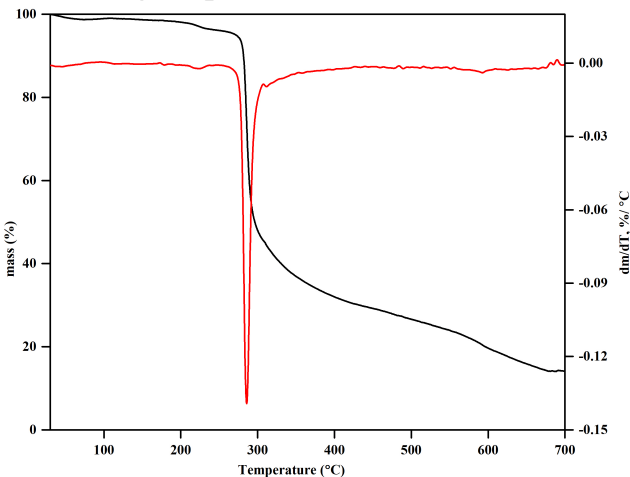


Fig. 5. The TG/DTG curves of dye **1b** at 10 °C min⁻¹

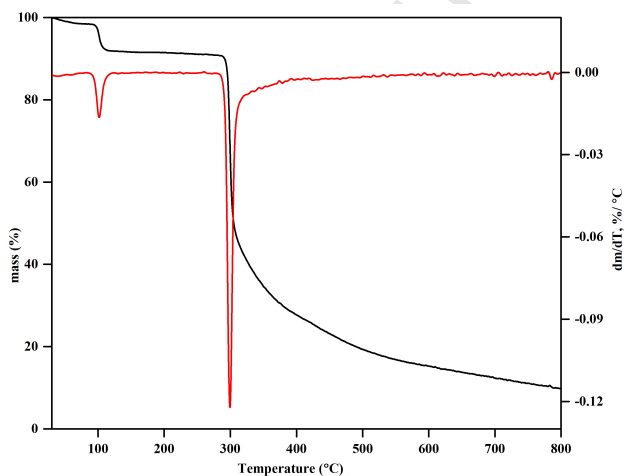


Fig. 6. The TG/DTG curves of dye **1c** at 10 °C min⁻¹

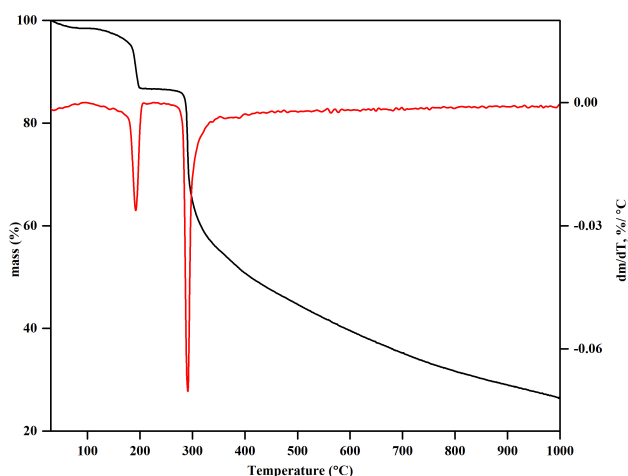


Fig. 7. The TG/DTG curves of dye **2a** at 10 °C min⁻¹

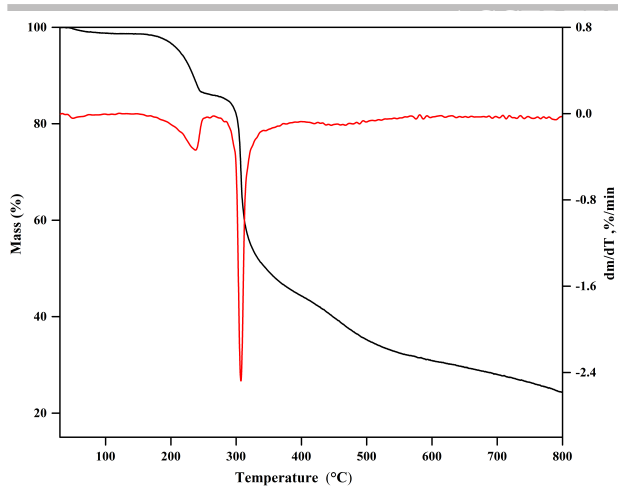


Fig. 8. The TG/DTG curves of dye **2b** at $10\text{ }^{\circ}\text{C min}^{-1}$

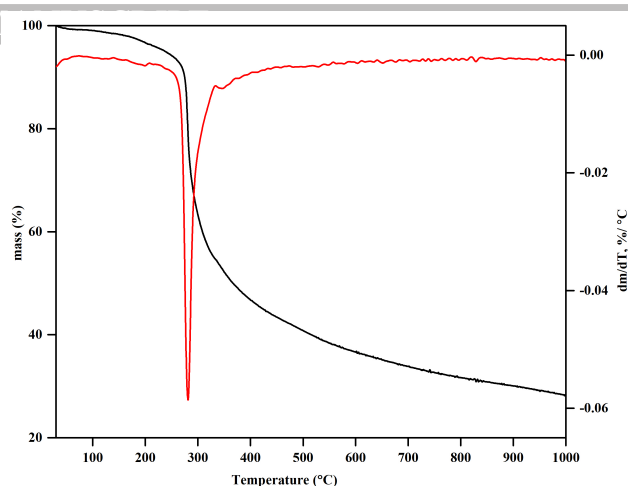


Fig. 9. The TG/DTG curves of dye **2c** at $10\text{ }^{\circ}\text{C min}^{-1}$

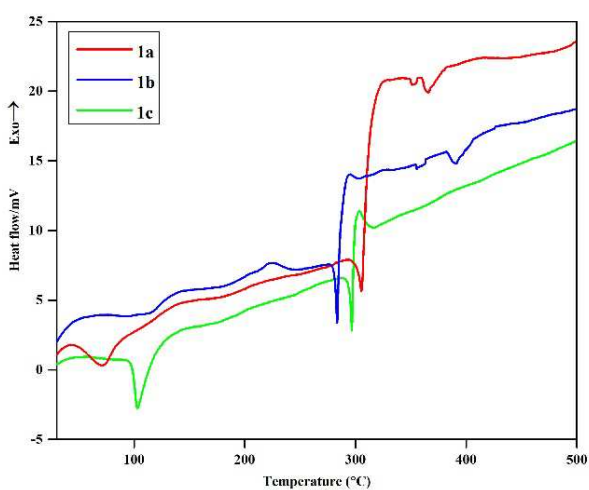


Fig. 10. DTA curves of **1a-c** dyes at $10\text{ }^{\circ}\text{C min}^{-1}$

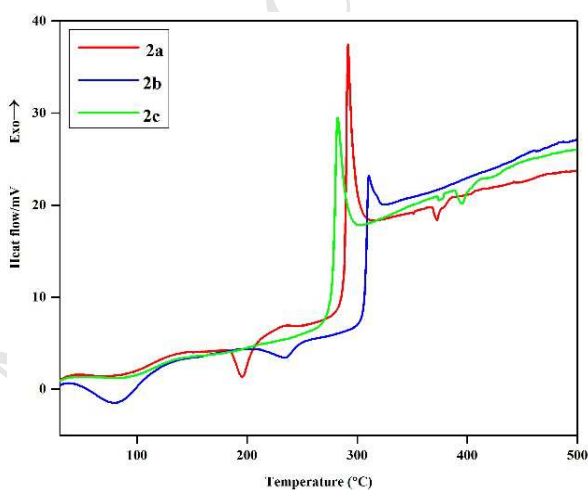


Fig. 11. DTA curves of **2a-c** dyes at $10\text{ }^{\circ}\text{C min}^{-1}$

The thermal characteristics of the synthesized dyes, which include corresponding degradation temperature intervals ($^{\circ}\text{C}$), the positions of DTG and DTA peaks (expressed in $^{\circ}\text{C}$), the mass loss values, as well as the total mass loss values (expressed in %) were summarized in Table 4.

Table 4. Thermal characteristics of arylazo pyridone dyes.

Compound	Degradation temperature interval (°C)	DTG peak value (°C)	Mass loss (%)	Total mass loss (%)	DTA peak value (°C)	
					Endo	Exo
1a	50 - 80	70.0	4	88	71.0	/
	277 - 400	305.6	63			
	400 - 800		21			
	180 - 270		4			
1b	270 - 425	285.8	65.9	82	283.6	294.0
	425 - 800		12.1			
	70 - 95		2			
1c	100 - 120	101.5	7.5	90	103.3	
	290 - 500	299.6	71.5			
	500 - 800		9			
2a	80		2	63	192.0	291.7
	130 - 195	192.1	10			
	275 - 700	291.6	51			
2b	/	85.0		72	234.6	311.1
	190 - 240	228.7	10			
	288 - 350	308.2	36			
	350 - 800		26.4			
2c	85		3	63	/	282.1
	260 - 320	280.7	37			
	320 - 700		23			

Based on these results (Fig. 4-11 and Table 4), it can be noticed that thermal stability does not only depend on the change of the cyano group into the amide on the pyridone ring, but also on the nature of the substituent at the *p*- position of the benzene ring of the coupling component. Considering dyes **1a-c**, the compound **1b** exhibits the lowest decomposition temperature (270 °C), even though it has the lowest structural steric hindrance (absence of substituent on *p*- position on phenyl ring), whereas the compound **1c** is of the highest one (290 °C) and the highest steric hindrance.

Taking into account the somewhat different shape of the thermo-analytical curves for dyes **2a-**

c compared to those present in dyes **1a-c**, the dye **2c** shows the lowest decomposition temperature (260 °C), while dye **2b** exhibits the highest (288 °C) (Table 4). The different thermal stabilities among various dye groups is probably the consequence of their chemical structure including diverse substituents that strongly affects this characterization issue. However, the slow and continuous decomposition of the molecular structure at several degradation steps (i.e. through three to four steps) with residues about 20% at the end of the process are observed as the general property of the studied dyes during degradation in an inert atmosphere (Table 4). As a result of these issues, the investigated dyes exhibit a complex thermo-analytical curves behavior. This probably can be attributed to their hardly decomposing properties related to corresponding structure (high value of molecular mass $\sim 300\text{g mol}^{-1}$). The different ways by which the dyes degrade depends upon the nature of substituent (hydroxy group or bromine atome). This phenomenon was related to the fact, whether the substituent is in *ortho*-, *meta*-, or *para*-position on the aromatic ring [45]. It was observed that if the substituent is in the *para*-position, the dye may show three steps of mass loss [45]. So, with respect to the temperature of degradation beginning, the following order can be obtained: dyes **1c** > **1a** > **1b**, and dyes **2b** > **2a** > **2c**. Different behavior of substituted dyes with -OH and -Br substituent is probably due to the different strength of the hydrogen bonds between the substituent on the phenyl ring and the hydrogen of the amide group or of the -NH group (hydrazone form).

Since that the initial degradation temperature after the release of adsorbed water molecules represents a measure of thermal stability [46], from above-indicated results, we can conclude that dyes **1a-c** exhibits higher thermal stability than dyes **2a-c**.

The enhanced thermal stability of dyes **1a-c** is supported by the fact that these dyes have more abilities to create intra-molecular hydrogen bonds between the oxygen of the carbonyl group and the proton from the amide group [47]. In addition, the thermal resistance was highest for more hindered dyes (Fig. 1), especially, for Br-substituted dye (about 290 °C).

The mass spectra of the obtained dyes are presented in Figures 12 a-f. Some characteristic degradation fragments are presented in Table 5. Other signals are probably derived from an intermediate or are formed by the interaction of the fragments. The corresponding chromatograms are presented in Figs. S1-S6 (*Supplementary material*).

Table 5. Characteristics m/z values and corresponding fragments.

Dye	m/z (experimental)	m/z (theoretical)	Chemical formula	Molecular weight, g/mol
1a	229.1	229.09	$C_{12}H_{11}N_3O_2$	229.24
	123.1	123.05	$C_6H_6N_2O^+$	122.13
	95.0	95.04	$C_5H_5NO^+$	95.10
	77.0	77.04	$C_6H_5^+$	77.11
1b	272.1	272.09	$C_{13}H_{12}N_4O_3$	272.26
	256.0	256.10	$C_{13}H_{12}N_4O_2$	256.27
	227.1	227.09	$C_{12}H_{11}N_4O^-$	227.25
	199.1	199.07	$C_{11}H_9N_3O$	199.21
	105.0	105.04	$C_6H_5N_2^+$	105.12
	94.1	94.03	$C_5H_4NO^-$	94.09
1c	281.1	281.0	$C_{11}H_{10}BrN_3O$	280.13
	184.9	184.95	$C_6H_4BrN_2^+$	184.02
	154.9	154.95	$C_6H_4Br^+$	156.00
	97.1	97.05	C_5H_7NO	97.12
2a	240.2	240.10	$C_{13}H_{12}N_4O$	240.1
	105.0	105.04	$C_6H_5N_2^+$	105.12
2b	254.2	254.08	$C_{13}H_{10}N_4O_2$	254.25
	91.7	91.04	$C_6H_5N^+$	91.11
2c	254.1	254.08	$C_{13}H_{10}N_4O_2$	254.25
	238.1	238.09	$C_{13}H_{10}N_4O$	238.25
	77.1	77.04	$C_6H_5^+$	77.11
	94.1	94.03	$C_5H_4NO^-$	94.09

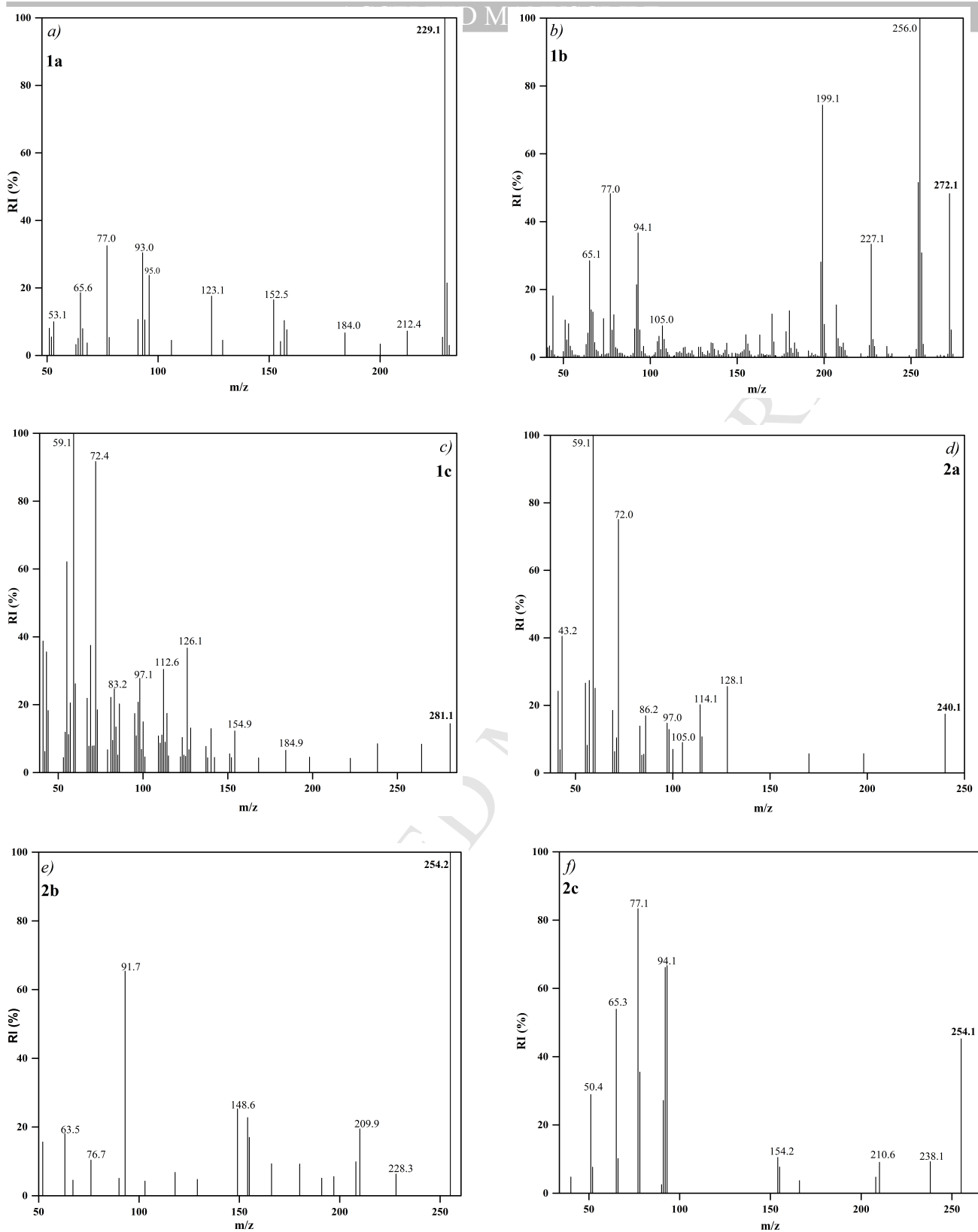


Fig. 12. Mass spectra fragmentation of dyes: a) **1a**, b) **1b**, c) **1c**, d) **2a**, e) **2b**, f) **2c**

The kinetic parameters at various heating rates (2.5, 5, 10 and 20 °C min⁻¹) for molecular structure degradation process that occurred at the second steps (250-400 °C) of all investigated dyes were determined using “model-free” kinetics.

The model-free analysis allows determining the activation energy of the reaction process without the assumption of a kinetic model for the process [48]. Also, the reaction type is usually not required to calculate the activation energy. The application of these methods is based on TGA curves recorded at 4 different heating rates.

Under linear heating condition, apparent activation energy and pre-exponential factor of the primary decomposition of all dyes are determined by two methods [49, 50]: Kissinger (1) and Ozawa (2) method. These methods are based on the changes in the exothermic peak temperature T_{max} , with changes in the heating rate β :

$$\log \frac{\beta}{T_{max}^2} = \log \frac{ZR}{E_a} - \frac{E_a}{2.303 \cdot RT_{max}} \quad (1)$$

$$\log \beta = \log \frac{ZE_a}{R} - 2.315 - 0.4567 \left(\frac{E_a}{RT_{max}} \right) \quad (2)$$

The activation energy and pre-exponential factor are evaluated from the linear dependence of $\log \beta$ versus $1/T_{max}$ as the slope and intercept, respectively.

To obtain the activation energy at different degrees of conversion, isoconversional integral methods Flynn-Wall-Ozawa (FWO) and Kissinger-Akahira-Sunose (KAS) were applied, according to the equation (3) and (4), respectively [51, 52].

$$\ln \beta = \ln \left(\frac{ZE_a}{Rf(\alpha)} \right) - 5.331 - 1.052 \frac{E_a}{RT} \quad (3)$$

$$\ln \left(\frac{\beta}{T^2} \right) = \ln \left(\frac{ZR}{E_a f(\alpha)} \right) - \frac{E_a}{RT} \quad (4)$$

β is the heating rate (2.5, 5, 10 and 20 °C min⁻¹), $f(\alpha)$ is the conversion function, Z – pre-exponential factor, E_a – activation energy (J mol⁻¹), R – gas constant (8.314 J mol⁻¹ K⁻¹), T – sample temperature in Kelvin.

The values of the activation energies can be derived from the slope $\ln\beta = f(1/T)$ for FWO method or from the slope $\ln(\beta/T^2) = f(1/T)$ for KAS method, without knowledge of $f(\alpha)$, by taking the values of β and T for different α values. The conversion degree dependence of temperature at different heating rates is presented in Fig. 13.

The influence of different temperatures regimes upon the thermal behavior of the investigated compound can provide kinetic parameters indicating change in the reaction pathway. The complexity of a stage can be expressed from the activation energy dependence on the conversion degree [33]. When E_a does not depend on α , only single reaction is involved and should be described by a unique kinetic triplet (E_a, Z, α). If activation energy changes with conversion degree, the process is complex. In the case of an increase in E_a with α , the process involves parallel reaction. In the case of a decrease in E_a with α and the concave shape of its evolution, the process has reversible stages. For decreasing convex shape, the process changes the limiting stage. The calculated $E_a(\alpha)$ dependence is presented in Fig. 14.

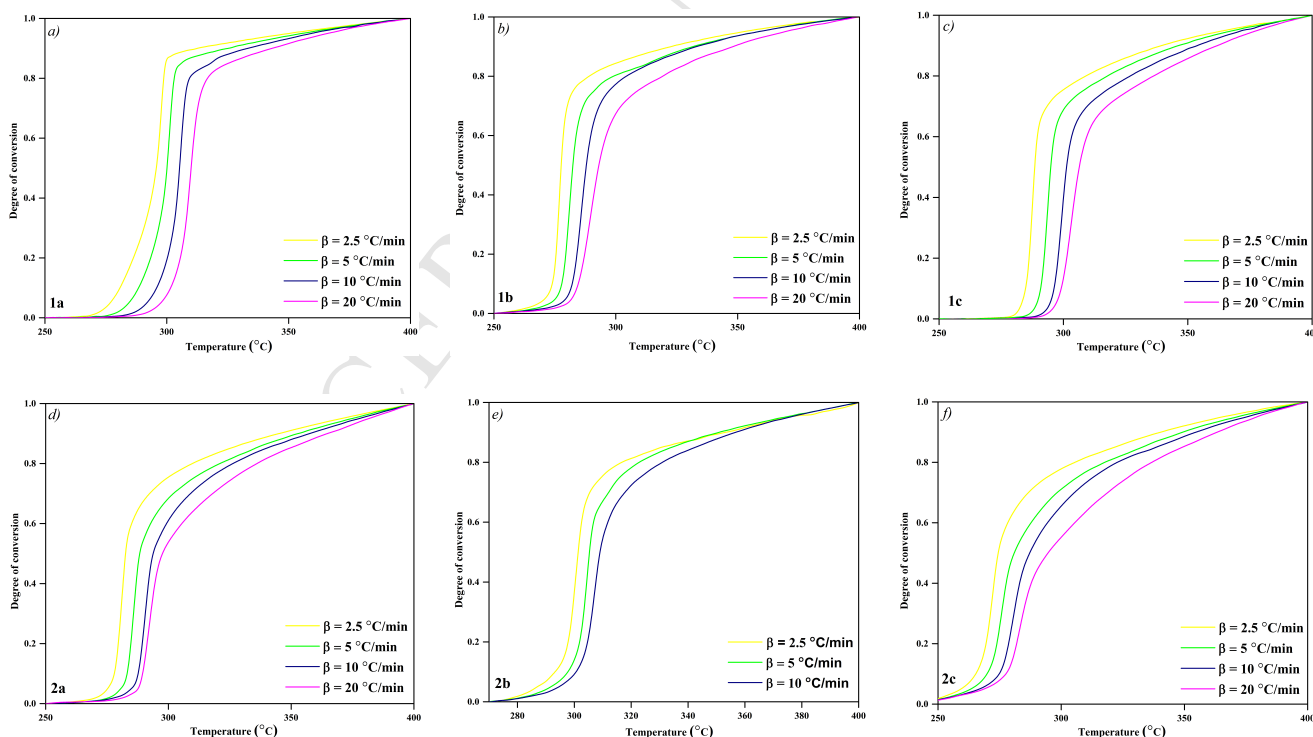


Fig. 13. The conversion degree of thermal decomposition vs. temperature for dyes: a)1a, b) 1b, c)1c, d)2a, e)2b, f)2c.

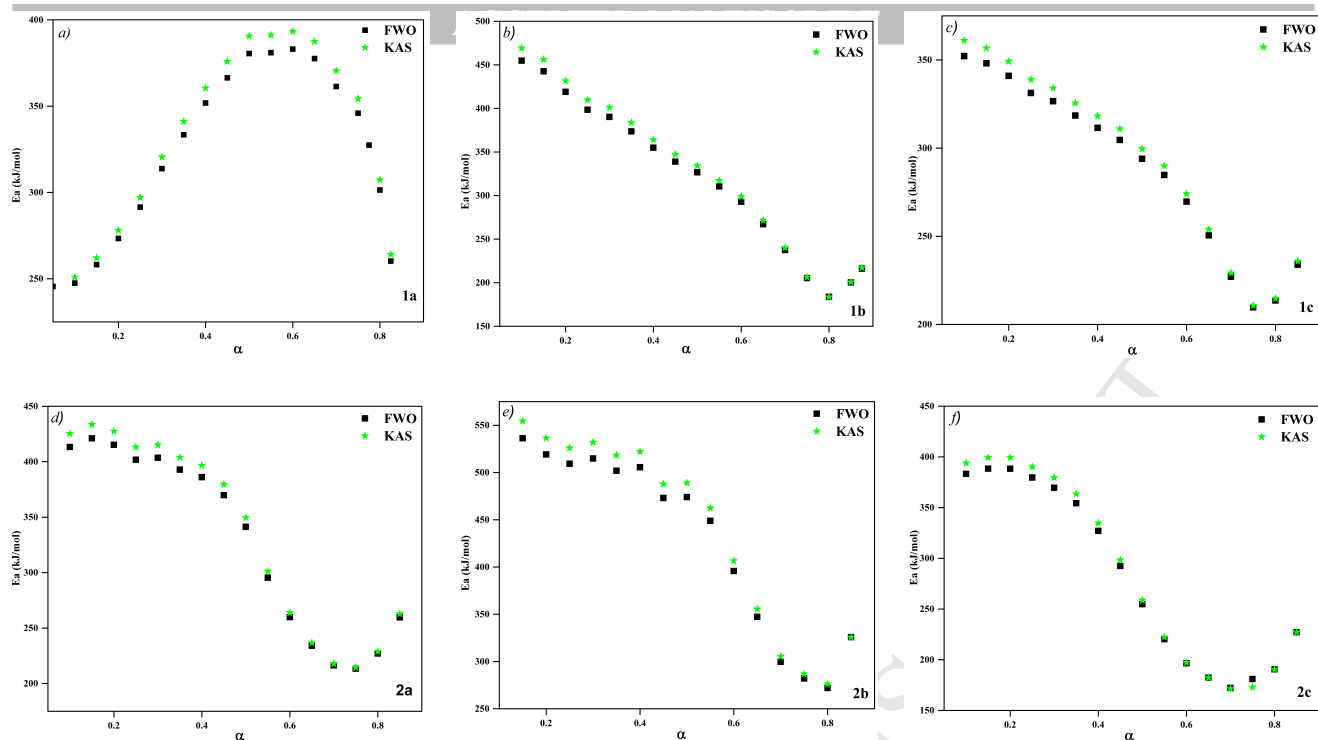


Fig. 14. Activation energies versus conversion degree for dyes: a) **1a**, b) **1b**, c) **1c**, d) **2a**, e) **2b**, f) **2c** using FWO and KAS methods.

For compound **1a** (Fig. 14a) increases in E_a value ($0.45 < \alpha < 0.65$) up to approximately 390 kJ mol^{-1} (FWO and KAS) can be attributed to the appearance of parallel reactions involving in the degradation process. These encompasses heterolytic splitting of azo bonds [53], where the phenol derivative in a form of $\text{C}_6\text{H}_6\text{ON}_2^+$ is releasing together with other charged chemical species. This is in accordance with the assumed degradation process (3.4).

Decreasing of E_a values for compounds **1b**, **1c**, **2a**, **2b** and **2c** with a conversion progression is attributed to the energy relaxation of this reaction stage, with released products which are instantly formed. However, this trend has a decreasing convex E-conversion shape (Fig 14b - f), so the degradation process changes the limiting stage [54]. A small increase in the E_a values in the conversion range $0.75 < \alpha < 0.9$ can be attributed to bond breaking events related to anhydrous dye structure and gaseous products releasing CO_2 and NO . The activation energy obtained by model free methods like the Kissinger, Ozawa, FWO and KAS are comparable and in good agreement.

Table 6. The value of E_a and Z using Kissinger and Ozawa method for dyes 1a-c and 2a-c

Compound	Kissinger method		Ozawa method	
	E_a , kJ/mol	Z , min ⁻¹	E_a , kJ/mol	Z , min ⁻¹
1a	456.06 (R=0.996)	2.21E+41	442.74 (R= 0.996)	3.85E+40
1b	408.33 (R=0.998)	2.34E+38	397.03 (R=0.998)	4.72E+37
1c	346.64 (R=0.979)	5.61E+31	338.57 (R=0.979)	1.63E+31
2a	474.69 (R=0.942)	2.11E+55	442.46 (R=0.940)	6.21E+41
2b	580.16 (R=0.978)	3.67E+63	542.48 (R=0.978)	6.77E+49
2c	483.65 (R=0.980)	8.78E+56	451.14 (R=0.979)	2.56E+43

Table 7. Kinetics and thermodynamics parameters value calculated by FOW and KAS methods for **1a**

α	FWO				KAS			
	E_a (kJ/mol)	ΔH (kJ/mol)	ΔG (kJ/mol)	ΔS (kJ/mol)	E_a (kJ/mol)	ΔH (kJ/mol)	ΔG (kJ/mol)	ΔS (kJ/mol)
0.15	258.18	253.55	149.43	0.182	262.13	257.50	149.36	0.189
0.2	273.32	268.67	149.16	0.209	278.02	273.37	149.08	0.217
0.25	291.47	286.80	148.85	0.241	297.08	292.41	148.76	0.251
0.3	313.79	309.09	148.50	0.281	320.52	315.84	148.40	0.293
0.35	333.41	328.71	148.22	0.316	341.14	336.44	148.11	0.329
0.4	351.80	347.08	147.96	0.348	360.47	355.76	147.84	0.364
0.45	366.40	361.68	147.77	0.374	375.82	371.09	147.65	0.391
0.5	380.43	375.70	147.59	0.399	390.56	385.83	147.46	0.417
0.55	380.99	376.25	147.58	0.400	391.14	386.40	147.46	0.418
0.6	383.04	378.29	147.56	0.403	393.28	388.54	147.43	0.422
0.65	377.51	372.76	147.63	0.394	387.46	382.71	147.50	0.412
0.7	361.39	356.64	147.83	0.365	370.49	365.74	147.71	0.382
0.75	345.94	341.19	148.04	0.338	354.23	349.48	147.93	0.353
0.8	301.39	296.64	148.70	0.259	307.35	302.59	148.60	0.269

Table 8. Kinetics and thermodynamics parameters value calculated by FOW and KAS methods **2a**

α	FWO				KAS			
	Ea (kJ/mol)	ΔH (kJ/mol)	ΔG (kJ/mol)	ΔS (kJ/mol)	Ea (kJ/mol)	ΔH (kJ/mol)	ΔG (kJ/mol)	ΔS (kJ/mol)
0.15	421.04	416.45	142.38	0.494	433.57	428.98	142.25	0.517
0.2	415.22	410.62	142.45	0.484	427.44	422.84	142.31	0.506
0.25	401.73	397.13	142.60	0.459	413.24	408.64	142.47	0.480
0.3	403.55	398.95	142.58	0.462	415.15	410.54	142.45	0.483
0.35	392.85	388.24	142.70	0.443	403.88	399.27	142.58	0.463
0.4	386.06	381.45	142.78	0.430	396.73	392.12	142.66	0.450
0.45	369.80	365.19	142.98	0.401	379.62	375.00	142.86	0.419
0.5	341.28	336.66	143.35	0.349	349.60	344.98	143.24	0.364
0.55	295.39	290.77	144.02	0.265	301.29	296.67	143.93	0.275
0.6	259.80	255.16	144.61	0.199	263.81	259.17	144.54	0.207
0.65	234.03	229.37	145.09	0.152	236.64	231.97	145.04	0.157
0.7	216.36	211.66	145.45	0.119	217.95	213.25	145.42	0.122
0.75	213.32	208.56	145.52	0.114	214.63	209.87	145.49	0.116
0.8	227.08	222.23	145.23	0.139	228.93	224.09	145.19	0.142

Enthalpy change, ΔH is the difference in energy level between the reagent and activated complex. The overall positive enthalpy change affirms that degradation of all obtained dyes is an endothermic reaction where heat energies readily absorbed by the system for breaking and formation of new chemical bonds. The difference in free Gibbs energy, ΔG , is the total increase in energy of a system during the approach of reagents and the formation of the activated complex. Generally, ΔG slightly grows with the progression of the conversion degree. A positive change in ΔG indicates *endergonic* reactions, i.e. non-spontaneous reactions. As degradation continues, more energy is required by the dyes to undergo conversion. Entropy change, ΔS , is the measure of the degree of disorder of a system where it explains the closeness of a system to its own thermodynamic equilibrium. As shown in Table 7 and 8, ΔS is high at initial conversional fraction but decreases as the conversion of sample increases. This indicates that as dyes are being degraded thermally, more reagents is being converted causing the unreacted reagent to decrease [55].

Thermal degradation of newly synthesized 5-(4-substitutedphenylazo)-3-amido-6-hydroxy-4-methyl-2-pyridone and previously synthesized 5-(4-substitutedphenylazo)-3-cyano-6-hydroxy-4-methyl-2-pyridone dyes, with different substituents in *para*-position of diazo components was investigated. The structures of the synthesized dyes were confirmed by NMR, FTIR, UV-Vis and XRD techniques. According to FTIR and NMR spectral data, dyes exist in the hydrazone form in the solid state and in DMSO-*d*₆. By application of simultaneous TGA-DTG technique with additional DTA analysis, the thermal stability and kinetic analysis of the degradation process of the investigated dyes were performed. The thermal analysis has shown that these compounds are stable up to 250 °C. As a result of this behavior, these dyes are suitable for use in high-temperature processes as photocopying and printing. Considering ultimate criteria related to the initial temperature for occurring of the primary degradation step, the following orders of thermal stability of dyes were established: dyes **1c** (Br-substituted) > **1a** (OH-substituted) > **1b** (unsubstituted), and dyes **2b** (unsubstituted) > **2a** (OH-substituted) > **2c** (Br-substituted). It was established that independently of a given substituent, the thermal stabilities of synthesized dyes are different. Generally, dyes **1a-c** are more stable than dyes **2a-c**.

It was found that different thermal stabilities of various dye groups are the consequence of their different chemical structures, including diverse substituents that strongly affects thermal analysis characterization issues. Complicated thermo-analytical curves for all dyes were identified. Results obtained from TGA, DTG and DTA in combination with GC-mass spectral fragmentation give proper consent. The dyes degradation occurs due to breaking of C=N bond (hydrazone form), except for dye **2b**, which degrade through the loss of N proton, followed by tautomerization to azo form and N=N bond breaking.

The kinetic parameters indicating change in the reaction pathways were established using various isoconversional (model-free) methods. Based on these results, it was found that the degradation mechanism of investigated arylazo pyridone dyes is complex. During the main

ACCEPTED MANUSCRIPT
degradation stage, the activation energy decreases with the conversion progress, indicating a complex degradation process.

Acknowledgments

Authors would like to acknowledge the financial support of Ministry of Education, Science and Technological Development of the Republic of Serbia under the Projects 45020, 172056 and 172013.

References

- [1] D.R. Waring, Heterocyclic dyes and pigments, *Comp. Het. Pigm.* 1 (1984) 317-346.
- [2] S. Manickasundaram, P. Kannan, Q.M.A. Hassan, P.K. Palanisamy, Azo dye based poly (alkyloxymethacrylate) and their spacer effect on optical data storage, *J. Mater. Sci. Mater. Electron.* 19 (2008) 1045-1053.
- [3] R.A. Toor, M.H. Sayyad, S.A.A. Shah, N. Nasr, F. Ijaz, M.A. Munawar, Synthesis, computational study and characterization of a 3-{{[2,3-diphenylquinoxalin-6-yl]diazanyl}}-4-hydroxy-2H-chromen-2-one azo dye for dye-sensitized solar cell applications, *J. Comput. Electron.* 17 (2018) 821-829.
- [4] H.F. Qian, X.L. Zhao, Y. Dai, W. Huang, Visualized fabric discoloration of bi-heterocyclic hydrazone dyes, *Dyes Pigm.* 143 (2017) 223-231.
- [5] D.Ž. Mijin, M. Baghbanzadeh, C. Reidlinger, C.O. Kappe, The microwave-assisted synthesis of 5-arylaazo-4,6-disubstituted-3-cyano-2-pyridone dyes, *Dyes Pigm.* 85 (2010) 73-78.
- [6] M.M.M. Raposo, M.C.R. Castro, M. Belsley, A.M.C. Fonseca, Pushpull bithiophene azo-chromophores bearing thiazole and benzothiazole acceptor moieties: Synthesis and evaluation of their redox and nonlinear optical properties, *Dyes Pigm.* 91 (2011) 454-465.
- [7] Y. Cheng, M. Zhang, H. Yang, F. Li, T. Yi, C. Huang, Azo dyes based on 8-hydroxyquinoline benzoates: Synthesis and application as colorimetric Hg²⁺-selective chemosensors, *Dyes Pigm.* 76 (2008) 775-783.
- [8] P. Kaur, S. Kaur, A. Mahajan, K. Singh, Highlyselective colorimetric sensor for Zn²⁺ based on hetarylazo derivative, *Inorg. Chem. Commun.* 11 (2008) 626-629.

- [9] X.L. Zhao, H.F Qian, W. Huang, Construction of benzothiazole/pyridone based bi-heterocyclic dyes and their Ni^{II} and Cu^{II} complexes, *Dyes Pigm.* 149 (2018) 796–803.
- [10] H. Valizadeh, A. Shomali, S. Nourshargh, R. M. Rezaei, Carboxyl and nitrite functionalized graphene quantum dots as a highly active reagent and catalyst for rapid diazotization reaction and synthesis of azo-dyes under solvent-free conditions, *Dyes Pigm.* 113 (2015) 522–528.
- [11] K. Gharanjig, M. Arami, H. Bahrami, B. Movassagh, N.M. Mahmoodi, S. Rouhani, Synthesis, spectral properties and application of novel monoazo disperse dyes derived from N-ester-1,8-naphthalimide to polyester, *Dyes Pigm.* 76 (2015) 684–689.
- [12] İ. Şener, N. Şener, M. Gür, Synthesis, structural analysis, and absorption properties of disperse benzothiazole derivative mono-azo dyes, *J.Mol. Struct.* 1174 (2018) 12–17.
- [13] Y. Zhang, Y. Liu, X. Ma, Ma X, B. Wang, H. Li, Y. Huang, C. Liu, An environmentally friendly approach to the green synthesis of azo dyes with aryltriazenes via ionic liquid promoted C-N bonds formation, *Dyes Pigm.* 158 (2018) 438–444.
- [14] Vinod kumar, J. Keshavayya, M. Pandurangappab, B.N. Ravi, Synthesis, Characterization and Electrochemical investigations of Azo dyes derived from 2-amino-6-ethoxybenzothiazole, *Chemical Data Collections* 17-18 (2018) 13–29.
- [15] A.J. Jarad, I.Y. Majeed, A.O. Hussein, Synthesis and spectral studies of heterocyclic azo dye complexes with some transition metals, *J. Phys. Conf. Series* 1003 (2018) 012021.
doi :10.1088/1742-6596/1003/1/012021
- [16] P.S. Jogi, J. Meshram, J. Sheikh, T.B. Hadda, Synthesis, biopharmaceutical characterization, and antimicrobial study of novel azo dyes of 7-hydroxy-4-methylcoumarin, *Med. Chem. Res.* 22 (2013) 4202–4210.
- [17] R. Sharma, R.K. Rawal, T. Gaba, N. Singla, M. Malhotra, S. Matharoo, T. R. Bhardwaj, Design, synthesis and ex vivo evaluation of colon-specific azo based prodrugs of anticancer agents, *Bioorganic Med. Chem. Lett.* 23 (2013) 5332–5338.

- [18] D.Ž. Mijin, B.B. Nedeljković, B.D. Božić, I. Kovrija, J. Lađarević, G. Ušćumlić, Synthesis, solvatochromism, and biological activity of novel azo dyes bearing 2-pyridone and benzimidazole moieties, Turk. J. Chem. 42 (2018) 896-907.
- [19] V.D. Vitnik, Ž.J. Vitnik, B.D. Božić, N.V. Valentić, S.P. Dilber, D.Ž. Mijin, G.S. Ušćumlić, Experimental and theoretical insight into the electronic properties of 4-aryl-5-aryloxy-3-cyano-6-hydroxy-2-pyridone dyes, Color. Technol. 1 (2016) 1-11.
- [20] B.D. Božić, A.S. Alimmari, D.Ž. Mijin, N. V. Valentić, G. S. Ušćumlić, Synthesis, structure and solvatochromic properties of novel dyes derived from 4-(4-nitrophenyl)-3-cyano-2-pyridone, J.Mol.Liq. 196 (2014) 61-68.
- [21] V.D. Vitnik, Ž.J. Vitnik, B.D. Božić, N.V. Valentić, S.P. Dilber, D.Z. Mijin, G.S. Ušćumlić, Experimental and theoretical insight into the electronic properties of 4-aryl-5-aryloxy-3-cyano-6-hydroxy-2-pyridone dyes, Color. Technol. 133 (2017) 223-233.
- [22] M.A. Zayed, G.G. Mohamed, M.A. Fahmey, Thermal and mass spectral characterization of novel azo dyes of *p*-acetoamidophenol in comparison with Hammett substituent effects and molecular orbital calculations, J. Therm. Anal. Calorim. 107 (2012) 763-776.
- [23] H. Deligoz, O. Ozen, G.C. Koyundereli, H. Cetisli, A study on the thermal behaviours of parent calix[4]arenes and some azocalix[4]arene derivatives, Thermochim. Acta 426 (2005) 33-38.
- [24] A.M.F. Oliveira-Campos, M.J. Oliveira, L.M. Rodrigues, M.M. Silva, M.J. Smith, Thermal analysis of a polymorphic azo dye derived from 2-amino-5-nitrothiazole, Thermochim. Acta 453 (2007) 52-56.
- [25] K. Wojceichowski, J. Szadowski, Thermal analysis of amide derivatives of N,N-dialkylaminobenzene, J. Therm. Anal. Calorim. 31 (1986) 297-303.
- [26] A. Tupys, J. Kalembkiewicz, Y. Ostapiuk, V. Matiichuk, O. Tymoshuk, E. Woznicka, L. Byczynski, Synthesis, structural characterization and thermal studies of a novel reagent 1-[(5-benzyl-1,3-thiazol-2-yl)diazenyl]naphthalene-2-ol, J. Therm. Anal. Calorim. 127 (2017) 2233–2242.

- [27] A. Moanta, A. Samide, P. Rotaru, C. Ionescu, B. Tutunaru, Synthesis and characterization of novel furoate azodye usingspectral and thermal methods of analysis, *J. Therm. Anal. Calorim.* 119 (2015) 1139–1145.
- [28] M.S. Masoud, E.A. Khalil, E. El-Sayed El-Shereafy, S.A. El-Enein, Thermal and electrical behaviour of nickel (II) and copper (II) complexes of 4-acetylamino-2-hydroxy-5-methylazobenzene, *J. Therm. Anal. Calorim.* 36 (1990) 1033-1038.
- [29] W.H. Mahmoud, M.M. Omar, F.N. Sayed, Synthesis, spectral characterization, thermal, anticancer and antimicrobial studies of bidentate azo dye metal complexes, *J. Therm. Anal. Calorim.* 124 (2016) 1071–1089.
- [30] M. Badea, R. Olar, E. Cristurean, D. Marinescu, A. Emandi, P. Budrugeac, E. Segal, Thermal stability of some azo-derivatives and their complexes Part 2. New azo-derivative pigments and their Cu (II) complexes, *J. Therm. Anal. Calorim.* 77 (2004) 815–824.
- [31] A.A. Joraid, A.A. Abu-Sehly, S.N. Alamri, S.Y. Al-Raqa, P.O. Shipmanc, P.R. Shipley, A.S. Abd-El-Aziz, Kinetics analysis of degradation of polynorbornene containing arylor hetaryl azo dye, *Thermochim. Acta* 529 (2012) 22– 24.
- [32] A.A. Joraid, S.N. Alamri, A.A. Abu-Sehly, S.Y. Al-Raqa, P.O. Shipman, P.R. Shipley, A.S. Abd-El-Aziz, Isothermal kinetics and thermal degradation of an aryl azo dye-containing polynorbornene, *Thermochim. Acta* 515 (2011) 38–42.
- [33] A. Rotaru, A. Moan, P. Rotaru, E. Segal, Thermal decomposition kinetics of some aromatic azomonoethers Part III. Non-isothermal study of 4-[(4-chlorobenzyl)oxy]-4'-chloroazobenzene in dynamic air atmosphere, *J. Therm. Anal. Calorim.*, 95 (2009) 161–166.
- [34] B. Janković, M. Marinović-Cincović, V. Jovanović, S. Samardžija-Jovanović, G. Marković, The comparative kinetic analysis of non-isothermal degradation process of acrylonitrile–butadiene and ethylene–propylene–diene rubber compounds. Part I, *Thermochim. Acta* 543 (2012) 295-303.
- [35] G.S. Ušćumlić, D.Ž. Mijin, N.V. Valentić, V.V. Vajs, B.M. Sušić, Substituent and solvent effects on the UV/Vis absorption spectra of 5-(4-substituted arylazo)-6-hydroxy-4-methyl-3-cyano-2 pyridones, *Chem. Phys. Lett.* 397 (2004) 148-153.

- [36] J. Dostanić, D. Mijin, G. Ušćumlić, D.M. Jovanović, M. Zlatar, D. Lončarević, Spectroscopic and quantum chemical investigations of substituent effects on the azo-hydrazone tautomerism and acid–base properties of arylazo pyridone dyes, *Spectrochim. Acta* 123 (2014) 37–45.
- [37] J.M. Mirković, B.Đ. Božić, D.R. Mutavdžić, G.S. Ušćumlić, D.Ž. Mijin, Solvent and structural effects on the spectral shifts of 5-(substitutedphenylazo)-3-cyano-6-hydroxy-1-(2-hydroxyethyl)-4-methyl-2-pyridones, *Chem. Phys. Lett.* 615 (2014) 62–68.
- [38] J.M. Dostanic, D.R. Loncarevic, P.T. Bankovic, O.G. Cvetkovic, D.M. Jovanovic, D.Z. Mijin, Influence of process parameters on the photodegradation of synthesized azo pyridone dye in TiO₂ water suspension under simulated sunlight, *J. Environ. Sci. Health. A Tox. Hazard. Subst. Environ.Eng.* 46 (2011) 70-79.
- [39] H. Song, K. Chen, H. Tian, Synthesis of novel dyes derived from 1-ethyl-3-cyano-6-hydroxy-4-methyl-5-amino-2-pyridone, *Dyes Pigm.* 53 (2002) 257-262
- [40] Q. Peng, M. Li, K. Gao, L. Cheng, Hydrazone-azo tautomerism of pyridone azo dyes: Part II: Relationship between structure and pH values, *Dyes Pigm.* 15(4) (1991) 263-274.
- [41] J. Mirković, J. Rogan, D. Poleti, V. Vitnik, Ž. Vitnik, G. Ušćumlić, D. Mijin, On the structures of 5-(4-, 3- and 2-methoxyphenylazo)-3-cyano-1-ethyl-6-hydroxy-4-methyl-2-pyridone: An experimental and theoretical study, *Dyes Pigm.* 104(2014) 160-168.
- [42] M.S. Aziz, H.M. El-Mallah, A.N. Mansour, Optical properties of azo dye (1-phenylazo-2-naphthol) thin films, *Eur. Phys. J. Appl. Phys.* 48 (2009) 20401
- [43] Y. Peng, X. Zhao, D. Xu, H. Qian, W. Huang, In situ metal-ion complexation and H₂O₂ oxidation for a pyridine-2,6-dione based disperse yellow dye, *Dyes and Pigments* 136 (2017) 559–568.
- [44] J. Mirković, J. Rogan, D. Poleti, V. Vitnik, Z. Vitnik, G. Ušćumlić, Dušan Mijin, On the structures of 5-(4-, 3- and 2-methoxyphenylazo)-3-cyano-1- ethyl-6-hydroxy-4-methyl-2-pyridone: An experimental and theoretical study, *Dyes Pigm.* 104 (2014) 160-168.
- [45] A.I. Burescu, I. Sava, M. Bruma, G. Lisa, Study of the thermal decomposition of some azopolyimides, *High Perf. Polym.* 26 (2014) 81-88.

- [46] H.M. Al-Maydama, A.G. El-Shekeil, A. Al-Karbouly, W. Al-Ikrimawy, Thermal degradation behavior of some poly [4-amino-2,6-pyrimidinothiocarbamate] metal complexes, Arab. J. Sci. Eng. 34 (2009) 67-75.
- [47] P.I. Nagy, Competing intramolecular vs. intermolecular hydrogen bonds in solution, Int. J. Mol. Sci. 15 (2014) 19562-19633.
- [48] E. Moukhina, Determination of kinetic mechanisms for reactions measured with thermoanalytical instruments, J. Therm. Anal. Calorim. 109 (2012) 1203-1214.
- [49] H.E. Kissinger, Reaction kinetics in differential thermal analysis, Anal. Chem. 29 (1957) 1702-1706.
- [50] T. Ozawa, A new method of analyzing thermogravimetric data. Bull. Chem. Soc. Jpn. 38 (1965) 1881-1886.
- [51] J.H. Flynn, L.A. Wall, A quick, direct method for the determination of activation energy from thermogravimetric data, J. Polym. Sci. B Polym. Lett. 4 (1966) 323-328.
- [52] T. Akahira, T. Sunose, Method of determining activation deterioration constant of electrical insulating materials, Res. Rep. Chiba Inst. Technol. (Sci. Technol.) 16 (1971) 22-31.
- [53] M. Gur, H. Kocaokutgen, M. Tas, Synthesis, spectral, and thermal characterisations of some azo-ester derivatives containing a 4-acryloyloxy group, Dyes and Pigments 72 (2007) 101-108.
- [54] S. Vyazovkin, N. Sbirrazzuoli, Isoconversional kinetic analysis of thermally stimulated processes in polymers, Macromol. Rapid Commun. 27 (2006) 1515-1532.
- [55] G.R. Mong, J.H. Ng, W.W.F. Chong, FN. Ani, S.S. Lam, C.T. Chong, Kinetic study of horse manure through thermogravimetric analysis, Chem. Eng. Trans. 72 (2019) 241-246.

Highlights

- TGA-DTG and DTA analysis of pyridone azo dyes were performed
- The thermal analysis has shown that dyes are stable up to 250°C
- The degradation occurs mainly due to breaking of C=N bond of hydrazone form
- The kinetic parameters indicated a change in the reaction pathways
- The investigated dyes are suitable for use in high-temperature processes